

## Use of a Linear Paul Trap to Study Random Noise-Induced Beam Degradation in High-Intensity Accelerators

Moses Chung\*

*Accelerator Physics Center, Fermi National Accelerator Laboratory, Batavia, Illinois 60510, USA*

Erik P. Gilson, Ronald C. Davidson, Philip C. Efthimion, and Richard Majeski

*Plasma Physics Laboratory, Princeton University, Princeton, New Jersey 08543, USA*

(Received 5 October 2008; published 9 April 2009)

A random noise-induced beam degradation that can affect intense beam transport over long propagation distances has been experimentally studied by making use of the transverse beam dynamics equivalence between an alternating-gradient (AG) focusing system and a linear Paul trap system. For the present studies, machine imperfections in the quadrupole focusing lattice are considered, which are emulated by adding small random noise on the voltage waveform of the quadrupole electrodes in the Paul trap. It is observed that externally driven noise continuously produces a nonthermal tail of trapped ions, and increases the transverse emittance almost linearly with the duration of the noise.

DOI: 10.1103/PhysRevLett.102.145003

PACS numbers: 52.59.Sa, 29.27.-a, 41.85.Ja, 52.27.Jt

Understanding the properties of intense ion beam propagation is of great importance for a wide variety of accelerator applications [1–3]. One critical but unavoidable problem in high-intensity accelerators is the presence of undesired random noise due to machine imperfections, and its influence on the long-time-scale beam dynamics [4–6]. Usually, random noise in the machine components acts as a continuous supply of free energy to the beam [4,5,7,8]. Consequently, the associated beam degradation defines the practical and/or economic tolerances in the machine design and operation [3,9]. In transforming random noise effects into emittance growth, the action of the nonlinear space-charge force plays a critical role [8]. Hence, it is increasingly important to understand the effects of random noise on long-distance beam propagation with moderate space-charge forces. From various multiparticle simulations with both space-charge and random noise effects, considerable progress has been made in developing an improved understanding of the random noise-induced beam degradation [5,6,8,10–12]. However, experimental verification of these effects has been somewhat limited due to the lack of dedicated experimental facilities that allow the study of long-time-scale phenomena.

The Paul Trap Simulator Experiment (PTSX), which is a linear Paul trap [13] that can experimentally simulate the nonlinear transverse dynamics of intense beam propagation over large equivalent distances through an alternating-gradient (AG) transport lattice [14,15], provides a compact and flexible laboratory facility for the experimental investigation of random noise effects. The idea of using a linear Paul trap confining a pure ion plasma to study intense beam propagation was proposed by Davidson *et al.* [14] and by Okamoto and Tanaka [16]. The physics equivalence between the AG system and the linear Paul trap system, including the self-field forces, is described in detail in Ref. [14]. The amplitude of the oscillating voltage wave-

form applied to the central electrodes in the PTSX device corresponds to the quadrupole focusing gradient in an AG lattice system. Hence, by slightly modifying the voltage amplitude  $V_{0\max}$  with the relative error limit  $\Delta_{\max}$  in every half-focusing period, we can simulate the effect of randomly distributed quadrupole focusing gradient errors in the actual transport channel.

The PTSX device [15] is constructed from a 2.8 m-long,  $r_w = 10$  cm-radius, gold-plated stainless steel cylinder (Fig. 1). The cylinder is divided into two 40 cm-long end cylinders and a  $2L = 2$  m-long central cylinder. All cylinders are azimuthally divided into four  $90^\circ$  sectors so that when an oscillating voltage  $V_0(t)$  is applied with alternating polarity on adjacent segments, the resulting electric field becomes an oscillating quadrupole field near the trap axis. This quadrupole electric field exerts a ponderomotive force that confines the pure ion plasma transversely. To trap the plasma axially, the two end electrodes are biased to a

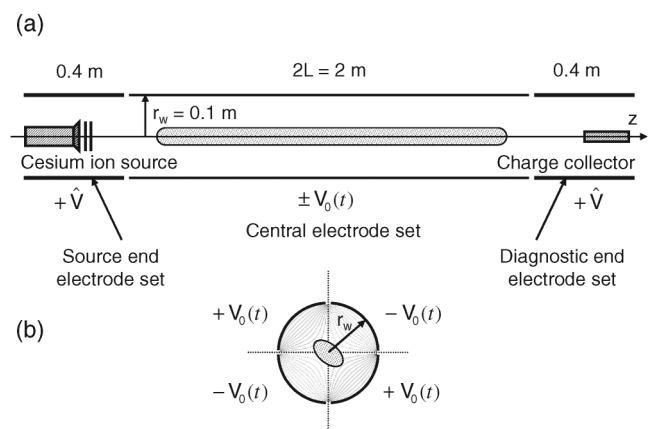


FIG. 1. Schematic of the PTSX device showing: (a) side view of the quadrupole electrodes, cesium ion source, and charge collector, and (b) end view of the central electrode set.

constant positive voltage  $+\hat{V}$  after the charge bunch is injected into the central section. The cesium ion source is located on the trap axis near the center of one of the short electrode set so that ion injection is not affected by the fringe fields. The charge collector is mounted on a linear motion feedthrough at the other end of the short electrode set, and can be moved in the transverse direction along a null of the applied potential. Through the sensitive electrometer with LABVIEW interface, the radial ion charge profiles can be measured accurately to as low as the 1 fC range, which is adequate to detect the formation of halo particles. The PTSX device manipulates the charge bunch using an inject-trap-dump-rest cycle, and the one-component plasmas created in the trap are highly reproducible [15]. A sinusoidal waveform  $V_0(t) = V_{0\max} \sin(2\pi f_0 t)$  is applied by an arbitrary function generator. Random noise is excited through another LABVIEW interface which samples a uniformly distributed random number  $\delta$  in the range  $|\delta| \leq \Delta_{\max}$ , and adjusts  $V_{0\max}$  to  $V_{0\max}(1 + \delta)$  in every half-focusing period  $1/2f_0$ . Application of the noise signal begins after the injected ion bunch becomes sufficiently stabilized (typically in about 12 ms), and ends before the dumping stage begins. In the dumping stage, most of the trapped ions are collected within 2 ms without significant changes in the radial density profile. Since the collected charge is necessarily averaged over many focusing periods during the dumping process, the value of the rms radius calculated from the measured radial profile can be interpreted as the rms radius of the beam in the smooth-focusing approximation [17]. In order to minimize the effects of neutral collisions on the plasma behavior, the base pressure of PTSX is kept below  $5 \times 10^{-9}$  Torr, and the trapped plasma is collisionless to very good approximation. The vacuum phase advance used in this experiment is  $\sigma_v = 52^\circ$ , which is considerably below the envelope instability limit [17].

In intense beams, the relative importance of space-charge effects can be described in terms of the normalized intensity parameter  $\hat{s} = \omega_p^2(0)/2\omega_q^2$  [17], where  $\omega_p^2(r) = n(r)q^2/m\epsilon_0$  is the plasma frequency squared, and  $\omega_q$  is the average smooth-focusing frequency of the beam particles' transverse oscillations in the applied focusing field. Here,  $\epsilon_0$  is the permittivity of free space,  $r$  is the radial distance from the beam axis, and  $q$  and  $m$  are the ion charge and mass, respectively. The radial ion density profile  $n(r)$  is related to the total axially integrated charge  $Q(r)$  through the collector plate centered at radius  $r$  by  $n(r) \approx Q(r)/q\pi r_c^2 L_p$ . Here,  $r_c$  is the size of the circular collecting plate and  $L_p$  is the plasma length. The PTSX device covers the operating range of  $0 < \hat{s} < 0.8$  by controlling the amount of charge injected by adjusting the voltages on the emitter surface, acceleration grid, and deceleration grid of the ion source [15]. In performing the actual experiments on random noise effects, however, it is important to minimize any other sources of beam state change that might be comparable to the random noise effects, such as

injection beam mismatch, and two-stream interactions [18], which become more significant for higher values of  $\hat{s}$ . Hence, for the experiments presented in this study, we use a moderately low space-charge-density beam ( $\hat{s} \sim 0.2$ , or equivalently, effective tune depression [19]  $\nu/\nu_0 \sim 0.95$ ) that has been carefully optimized through the injection scheme described in Ref. [18]. If the moderately low space-charge-density beam has a thermal equilibrium distribution, it is expected that the beam has a Gaussian-like radial profile [19]. Indeed, Fig. 2 shows that the measured radial charge profile is approximately a Gaussian function of  $r$  with temperature comparable to the thermal temperature of the cesium ion source ( $\sim 1000^\circ\text{C}$ ), indicating the validity of the assumption of a thermal-equilibrium-like beam. The optimized plasma is obtained 12 ms after the ion injection is completed, and can be held in a thermal-equilibrium-like state for about 38 ms (Fig. 2), which is equivalent to quiescent beam propagation over about 2280 full AG focusing periods for  $f_0 = 60$  kHz. Here, the transverse defocusing space-charge force is about 10% of the applied transverse focusing force, and other possible sources of thermalization of the free energy, such as collisions with the background gas and nonlinearities in the applied focusing force [14], are estimated to be negligibly small for the present experimental conditions. In addition, the number of error samples is also an important factor for obtaining good statistics in the experimental data [10]. In multiparticle simulations, the number of error samples has been chosen as small as 20 [11], or as large as 500 [5], depending on the computation time and required accuracy for the quantitative analysis. For the initial experiments reported in this study, we use 20 error samples for a given noise amplitude and duration.

Since the error limit  $\Delta_{\max}$  in the focusing force is typically only a few percent, any possible changes due to the random noise in the global quantities such as the line density  $N = \int_0^{r_w} n(r)2\pi r dr$ , the mean-squared radius  $R_b^2 = (1/N) \int_0^{r_w} n(r)2\pi r^3 dr$ , the effective transverse temperature  $\bar{T}_\perp$ , and the average transverse emittance  $\epsilon$ , will

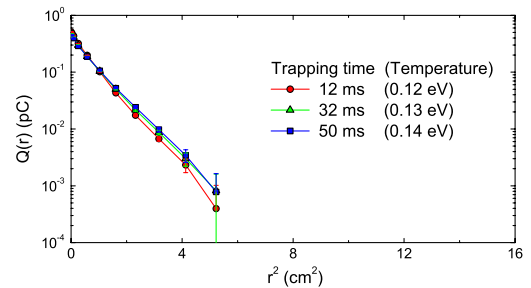


FIG. 2 (color online). Measured radial charge profiles  $Q(r)$  of trapped plasma ( $\hat{s} \sim 0.2$ ) without applied noise. The charge bunch is maintained in the quasiequilibrium state for about 38 ms with a slight increase in the effective transverse temperature [calculated from Eq. (1)]. A straight line in the log of  $Q(r)$  versus  $r^2$  plot indicates that the radial profile is a Gaussian function of  $r$ .

take place quite slowly. In this case, we can assume that the beam is in a quasiequilibrium state, which means that the average transverse focusing force balances both the thermal pressure force of the plasma and the space-charge force over a slow time scale. Therefore, the global force balance equation can be expressed approximately as [17]

$$m\omega_q^2 R_b^2 = 2\bar{T}_\perp + \frac{Nq^2}{4\pi\epsilon_0}, \quad (1)$$

and the evolution of the effective average transverse emittance can be approximated by

$$\epsilon(t) = 2R_b \left( \omega_q^2 R_b^2 - \frac{Nq^2}{4\pi\epsilon_0 m} \right)^{1/2}. \quad (2)$$

Simulation studies [20] using the WARP 2D code [21] indicate that the free energy available from the noise-induced envelope oscillations is converted into an increase in the rms beam size through the action of the nonlinear space-charge force for similar experimental condition as in the present study. Hence, Eq. (2) is expected to be a valid approximation which allows us to estimate the approximate emittance growth due to the random noise, simply by using the values of  $N$  and  $R_b$  measured in the experiments. However, when there exists a significant population of low-density halo particles below the detection limit ( $\approx 1$  fC) of the charge collector, then the emittance calculated from Eq. (2) necessarily underestimates the actual mean transverse emittance. Particles far away from the beam core ( $> \sqrt{2}R_b$ ) are of course weighted more heavily in calculating the emittance in the simulations [12,21].

To characterize the statistical properties of the beam response to the random noise, we make use of the on-axis charge  $Q(r=0)$ . Figure 3 shows the time history of the statistical average  $\mu$  and the standard deviation  $\sigma$  of the on-axis charge computed over an ensemble of 20 random error samples. The average of the on-axis charge decays almost linearly with the duration of the noise up to 25 ms. After 25 ms, the decay rate becomes somewhat rapid, which is likely related to the production of halo particles (see Fig. 4) and the resultant enhanced particle loss. Because of the relatively small number of error samples, it is not clear if the beam response is a random-walk-like diffusion process ( $\sigma \propto t^{1/2}$ ). However, the general tendency is that the standard deviation of the on-axis charge increases with time, which strongly suggests that the fluctuations in the on-axis charge measurements originate from the applied noise rather than from instrumental uncertainties (i.e.,  $\sigma \approx \text{const.}$ ) or statistical fluctuations (i.e.,  $\sigma \propto \sqrt{\mu}$ ) [22].

When the beam is in a thermal-equilibrium-like state, the on-axis density can be represented by a single parameter that effectively characterizes the variation of the equilibrium density profile from one error sample to another for a given noise amplitude and duration [19]. Hence, except for the case where there is a significant departure from the thermal equilibrium state, we can infer the rms radius  $R_b$

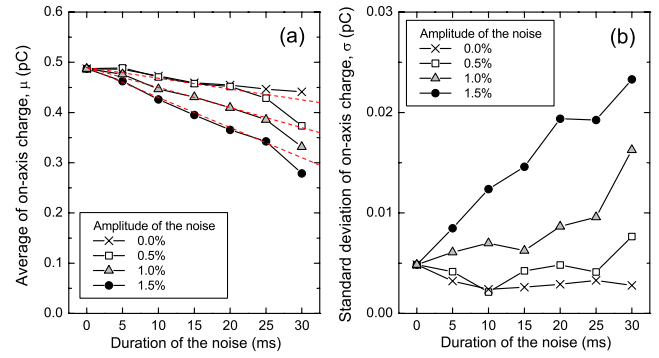


FIG. 3 (color online). Time history of (a) the statistical average, and (b) the standard deviation of the on-axis charge computed over an ensemble of 20 random error samples. Dashed lines are drawn to indicate linear behavior of on-axis charge decay.

averaged over the ensemble of 20 error samples by using the statistical properties of the on-axis charge summarized in Fig. 3. By measuring a single radial profile for a given noise amplitude and duration, with a specified error sample that gives  $Q(r=0) \approx \mu$ , we can effectively obtain the ensemble-averaged  $R_b$ . Otherwise, it would be necessary to measure the radial profile for every error sample, which requires 360 independent radial profile measurements to scan the entire parameter range, and would be vulnerable to any drift in the experimental conditions. In the present study, the processes of choosing an appropriate error sample and measuring the corresponding radial profile have

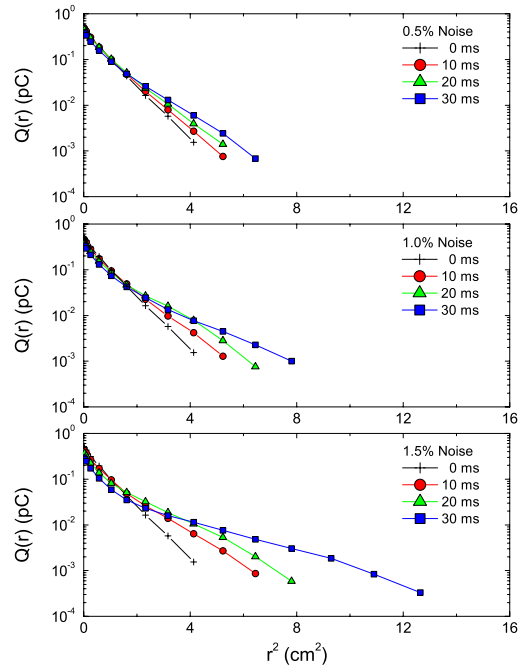


FIG. 4 (color online). Measured radial charge profiles  $Q(r)$  with different noise amplitudes and durations. Initially, the trapped plasma is in a thermal-equilibrium-like state, for which  $Q(r)$  is a straight line in the log versus  $r^2$  plot.

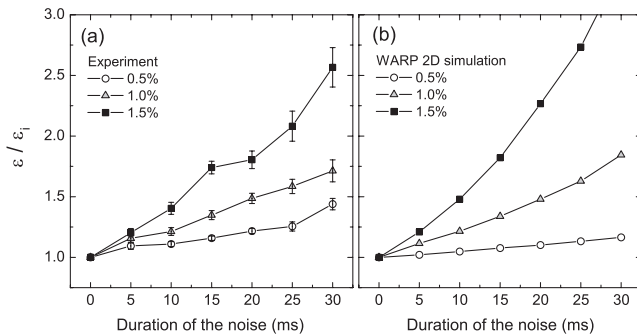


FIG. 5. The emittance growth is estimated from (a) radial profile measurements, and (b) WARP 2D PIC simulations. The emittance is calculated from Eq. (2), and is normalized to its initial value  $\epsilon_i$ . Note that error bars result from the instrumental uncertainties in the radial profile measurements. For the WARP simulations, 20 random error samples are used to calculate the ensemble-averaged emittance.

been performed in 5 ms intervals (300 focusing periods) with three different noise amplitudes, which require only 18 independent radial profile measurements. In Fig. 4, the measured radial charge profiles are shown in 10 ms intervals rather than 5 ms intervals to indicate the evolution of the low-density tail more clearly.

Consistent with simulations using the WARP 2D code, we observe a continuous emittance growth which is approximately linear with the duration of the noise (Fig. 5). For the case where  $\Delta_{\max} = 1.5\%$ , however, the experimentally determined emittance is somewhat underestimated after a noise duration of 15 ms. This is most likely due to the formation of a significant halo population under the detection limit ( $\sim 1$  fC) of the charge collector, which is too low to be measured in the experiment, but contributes considerably in the simulations. The formation of a significant halo population is apparent in Fig. 4. On the other hand, for the case with  $\Delta_{\max} = 0.5\%$ , the experimentally estimated emittance in Fig. 5 has a slightly larger value than the simulation results, which is likely due to the intrinsic noise present in the PTSX device, such as jitter in the voltage waveform or mechanical vibrations from the vacuum pump.

In this study, we have presented experimental verification of the random noise-induced beam degradation theoretically expected in high-intensity accelerators. The amplitude of the noise used to emulate machine imperfection effects in this study may be somewhat larger than the actual tolerance limits [5]. This is a practical compromise to overcome the difficulty of measuring small changes in charge signals in the PTSX device. Nonetheless, in modern high-intensity accelerators, loss of only a few particles per meter can cause radioactivation that would preclude routine hands-on maintenance [4]. Therefore, it is highly relevant to verify the validity of numerical tools and to test the physics models for beam loss in experiments with parameters even somewhat beyond the actual tolerance limits. Future experiments with different space-charge

strength are expected to provide a more detailed understanding of the role of space-charge force in random noise-induced beam degradation.

This research was supported by the U. S. Department of Energy.

\*The research was carried out at Plasma Physics Laboratory while the author was at Princeton University.

- [1] R. C. Davidson and H. Qin, *Physics of Intense Charged Particle Beams in High Energy Accelerators* (World Scientific, Singapore, 2001), Chap. 1, and references therein.
- [2] M. Reiser, *Theory and Design of Charged Particle Beams* (Wiley-VCH, Weinheim, 2008), 2nd ed., Chap. 7.
- [3] T. Wangler, *RF Linear Accelerators* (Wiley-VCH, Weinheim, 2008), 2nd ed., Chap. 12.
- [4] C. L. Bohn and I. V. Sideris, *Phys. Rev. Lett.* **91**, 264801 (2003).
- [5] F. Gerigk, *Phys. Rev. ST Accel. Beams* **7**, 064202 (2004).
- [6] J. Qiang, R. D. Ryne, B. Blind, J. H. Billen, T. Bhatia, R. W. Garnett, G. Neuschaefer, and H. Takeda, *Nucl. Instrum. Methods Phys. Res., Sect. A* **457**, 1 (2001).
- [7] I. V. Sideris and C. L. Bohn, *Phys. Rev. ST Accel. Beams* **7**, 104202 (2004).
- [8] G. Franchetti and I. Hofmann, in *Proceedings of 2002 European Particle Accelerator Conference, Paris, France* (EPS-IGA/CERN, Geneva, 2002), p. 1353.
- [9] F. Gerigk, in *Proceedings of the 29th ICFA Advanced Beam Dynamics Workshop* (AIP, New York, 2003), p. 61.
- [10] D. V. Gorelov and P. N. Ostroumov, in *Proceedings of the 1998 International Linear Accelerator Conference, Chicago, USA* (ANL, Argonne, 1998), p. 654.
- [11] M. Ikegami, T. Ohkawa, Y. Kondo, and A. Ueno, in *Proceedings of 2004 International Linear Accelerator Conference, Lubeck, Germany* (DESY/GSI, 2004), p. 345.
- [12] P. S. Yoon, W. Chou, and C. L. Bohn, in *Proceedings of the 2005 Particle Accelerator Conference, Knoxville, Tennessee* (IEEE, Piscataway, NJ, 2005), p. 117.
- [13] W. Paul and H. Steinwedel, *Z. Naturforsch.* **8A**, 448 (1953).
- [14] R. C. Davidson, H. Qin, and G. Shvets, *Phys. Plasmas* **7**, 1020 (2000).
- [15] E. P. Gilson, R. C. Davidson, P. C. Efthimion, and R. Majeski, *Phys. Rev. Lett.* **92**, 155002 (2004).
- [16] H. Okamoto and H. Tanaka, *Nucl. Instrum. Methods Phys. Res., Sect. A* **437**, 178 (1999).
- [17] See, for example, Chaps. 3 and 5 of Ref. [1].
- [18] M. Chung, E. P. Gilson, M. Dorf, R. C. Davidson, P. C. Efthimion, and R. Majeski, *Phys. Rev. ST Accel. Beams* **10**, 014202 (2007).
- [19] R. C. Davidson and H. Qin, *Phys. Rev. ST Accel. Beams* **2**, 114401 (1999).
- [20] M. Chung, Ph.D. thesis, Princeton University, Princeton, NJ, 2008, p. 179.
- [21] A. Friedman, D. P. Grote, and I. Haber, *Phys. Fluids B* **4**, 2203 (1992).
- [22] P. R. Bevington and D. K. Robinson, *Data Reduction and Error Analysis for the Physical Sciences* (McGraw-Hill, New York, 1992).